Journal of Applied Polymer Science

Fabrication of PFO-DBT:OXCBA nanostructured composite via hard template

Muhamad Saipul Fakir,[1] Azzuliani Supangat,[2] Khaulah Sulaiman[2]

[1]Department of Physics, Faculty of Science, University of Malaya, Kuala Lumpur 50603, Malaysia

[2]Department of Physics, Faculty of Science, Low Dimensional Materials Research Centre, University of Malaya, Kuala Lumpur 50603, Malaysia

Correspondence to: A. Supangat (E-mail: azzuliani@um.edu.my)

ABSTRACT: Poly[2,7-(9,9-dioctylfluorene)-*alt*−4,7-*bis*(thiophen-2-yl)benzo-2,1,3-thiadiazole] (PFO-DBT) and *o*-xylenyl-C_{60}-bisadduct (OXCBA) nanostructured composite has been fabricated via the hard porous alumina template-directed method. Spin-coating technique at the spin rate of 1000 rpm is used to assist the infiltration of polymer solution into porous template. PFO-DBT nanotube is fabricated by replicating the porous alumina template before the formation of PFO-DBT:OXCBA nanostructured composite. Formation of nanostructured composite is completed once the infiltration of OXCBA solution into PFO-DBT nanotubes is achieved. Detailed results of morphological, structural, and optical properties of PFO-DBT nanostructures (nanorods and nanotubes) of different solution concentrations are reported. By tuning the optical properties of PFO-DBT nanostructures, the effect of solution concentration on the optical properties can be realized. The promising PFO-DBT nanotubes are chosen for the further fabrication of OXCBA:PFO-DBT nanostructured composite that acts as a core and shell, respectively. Although the nanostructured composite of PFO-DBT:OXCBA yield low light absorption intensity, the absorption spans the whole visible region and produce low optical energy gap. © 2016 Wiley Periodicals, Inc. J. Appl. Polym. Sci. **2016**, *133*, 44228.

KEYWORDS: composites; conducting polymers; morphology; nanostructured polymers; optical properties

Received 12 February 2016; accepted 28 July 2016

DOI: 10.1002/app.44228

INTRODUCTION

Organic semiconducting materials are currently used as the active layer of organic electronics devices such as organic solar cells (OSCs), organic field effect transistors (OFETs), and organic light emitting diodes (OLEDs).[1–4] Thiophene-based materials are one of the most promising materials that have been widely used in organic electronics devices and sensors as an active layer due to their great optical properties and low optical energy gap. Among these materials is poly[2,7-(9,9-dioctylfluorene)-*alt*−4,7-*bis*(thiophen-2-yl)benzo-2,1,3-thiadiazole] (PFO-DBT), which is known as an electron donor material. Realizing the great potential of optical properties of PFO-DBT, a number of studies have been undertaken to improve the synthesis of PFO-DBT in order to enhance its properties for future applications.[5–8] In the development of organic electronics devices, the main reason behind the extensive attention given to the organic semiconducting materials has much to do with its low optical energy gap. It has been reported that low optical energy gap of thiophene-based materials can yield a better performance of devices.[1,9,10] Some investigations made by researchers claiming that the performance of organic photovoltaic devices become more efficient due to the low optical energy gap.[11–13]

In most of the organic electronics devices, active layer composes of electron donor and electron acceptor plays a vital role in ensuring the enhanced performance of devices. Fullerene-based materials are the common electron acceptor used in solution processing devices. Its derivatives, fullerene *bis*-adducts such as OXCBA which consist of two solubilizing group possessed a lower lowest unoccupied molecular orbital (LUMO) than the LUMO level of fullerene-based PCBM.[14] In the case of organic solar cells, the lower LUMO level of an electron acceptor material give an advantages since the open-circuit voltage (V_{OC}) is proportional to the difference between the LUMO level of acceptor and highest occupied molecular orbital (HOMO) level of donor material. Therefore, incorporated the derivatives of fullerene-based material of lower LUMO level can increase the value of V_{oc}. Recent studies on utilising OXCBA as the acceptor material in photovoltaic device showed the increase in the open-circuit voltage from around 0.6 V to 0.8 V which leads to a better efficiency of the device.[15]

Intensive research studies have been performed to modify the structure of materials, for the improvement of device architectures, surface modifications, and fabrication processes. Integrating

the nanostructured composite materials of low optical energy gap as the active layer is one of the facile way to boost the performance of devices. Simulation work by Marsh *et al.* about the nanostructured organic photovoltaic realised that an idealized interdigitated structure could achieve overall efficiencies twice as high as blend.[16] Experimental work on the influence of nanomorphology of polymer-fullerene modification in a photovoltaic device was done by Chirvase *et al.*[17] The modification was done by varying the weight ratio of the acceptor material. As a result, the nanoclusters of acceptor material were formed and lead to formation of percolation paths and, therefore, improve the photocurrent. Since both simulation and experimental works show the benefits of introducing the nanostructure, studies on synthesizing the nanostructured PFO-DBT should be given more focuses and priorities before incorporating with the fullerene-based material.

One of the easiest and effective ways to synthesize the nanostructured composite materials in the large scale is via template-assisted method. Templating approach is a top-bottom nanoscale fabrication, which provides a good replication of template's diameter and thickness. A porous alumina of hard template can be used as a mould to replicate and fabricate the nanostructured composite materials. An average porous density of the template is 10^{11} pores/cm^2 with pore size varied from 10 nm to 100 μm.[18] Previously, works implementing the porous alumina of hard template have been done to synthesize the micro- and nanostructures such as nanocomposite,[19] nanoflowers,[20,21] nanorods,[22,23] and nanotubes.[23,24]

In the present work, spin coating technique is used to infiltrate the PFO-DBT solution of different solution concentrations into porous alumina template for the fabrication of PFO-DBT nanostructures. The high viscosity may affect the ability of the solution to infiltrate into the porous template. The presynthesized PFO-DBT nanotubes will then be used as a template for the OXCBA solution to infiltrate and form the core. Thus, this work will focus on the characterisation and fabrication of PFO-DBT:OXCBA nanostructured composite via hard template.

EXPERIMENTAL

Materials

Both organic semiconductor materials, poly[2,7-(9,9-dioctylfluorene)-*alt*-4,7-*bis*(thiophen-2-yl)benzo-2,1,3-thiadiazole] (PFO-DBT) (M_w = 10,000–50,000 (GPC)) and *o*-Xylenyl-C_{60}-bisadduct (OXCBA) (M_w = 928.92g/mol, purity = >99%) were purchased from LUMTEC (Hsin-Chu, Taiwan) and utilized without further purification. Chloroform (99% purity) was used as the solvent for solution preparation. Commercially available alumina template with 20 nm of top surface porous and 200 nm branched porous structure of 60 μm thickness was purchased from Whatman Anodisc.

Characterization Techniques

Characterisations of PFO-DBT nanostructures and PFO-DBT:OXCBA composites were performed using Field Emission Scanning Electron Microscopy (FESEM) (JEOL, JSM-7600F, Tokyo, Japan), High Resolution Transmission Electron Microscopy (HRTEM) (HITACHI HT7700, Krefeld, F.R. Germany), UV-Vis spectroscopy (Jasco V-750, Tokyo, Japan), Raman, and photoluminescence spectroscopy (Renishaw, Gloucestershire, UK).

Fabrication of PFO-DBT Nanostructures

PFO-DBT solution was deposited using spin coater. Three different solution concentrations of 5, 10, and 15 mg/mL were prepared by dissolving the corresponding weight of PFO-DBT powder in 1 mL of chloroform. The porous alumina template was placed on the spinning dish of a standard spin coater model WS-650MZ-23NPP (Laurell Tech. Corp., North Wales, PA) before spinning at constant spin rate and time of 1000 rpm and 30 s, respectively. The sample was then annealed in an oven at 60 °C for 10 min. The process of fabrication is simplified by the schematic diagram in Figure 1(A–E).

Fabrication of PFO-DBT:OXCBA Nanostructured Composite

OXCBA solution was prepared separately by dissolving 10 mg of its corresponding powder in 1 mL of chloroform to produce 10 mg/mL solution concentration. Two processing steps are involved in producing the PFO-DBT:OXCBA nanostructured composite, since the deposition of PFO-DBT and OXCBA solution need to be done separately. OXCBA solution was deposited on top of predeposited PFO-DBT using spin coater at the spin rate and spin time of 1000 rpm and 30 s, respectively. The sample was then annealed at 60 °C for 10 min to eliminate the residual. Template with the infiltrated PFO-DBT and OXCBA solution was then immersed in 3 *M* of sodium hydroxide (NaOH) to dissolve the template before being purified by the deionized water and leaving only the PFO-DBT nanostructures or PFO-DBT: OXCBA nanostructured composite. The fabrication process is simplified by the schematic diagram in Figure 1(F–I).

RESULTS AND DISCUSSION

Effect of Solution Concentration on PFO-DBT Nanostructures

The aim of this work is to demonstrate the fabrication of highly dense PFO-DBT nanostructures via the hard template-directed growth. Without the use of template, spin-coated polymer solution will usually spread out homogenously and cover the whole area of substrate, to form polymer thin film. Polymer solution will experience the centripetal force that helps the solution to spread out all over the substrate. During the spin coating process, the viscosity and surface tension of solution led to the occurrence of solution from being thrown and spilled out. Using the nanoporous substrate such as hard porous alumina template, a similar phenomenon of centripetal force, solution viscosity, and surface tension can be achieved during the spinning process. Solution will be spread and infiltrated into the porous media and dry instantly. Infiltration process will become easier with the assist of centripetal force since it could provide to the polymer's static or vibration. Rigorous infiltration of solution into the porous media is required for the fabrication of highly dense PFO-DBT nanostructures. Recent studies on the dependent of spin-coating rate on the formation of nanostructures have proven the importance of spin-coating technique in assisting the infiltration process. In addition, the fabrication of PFO-DBT nanostructures that obtained from the different spin

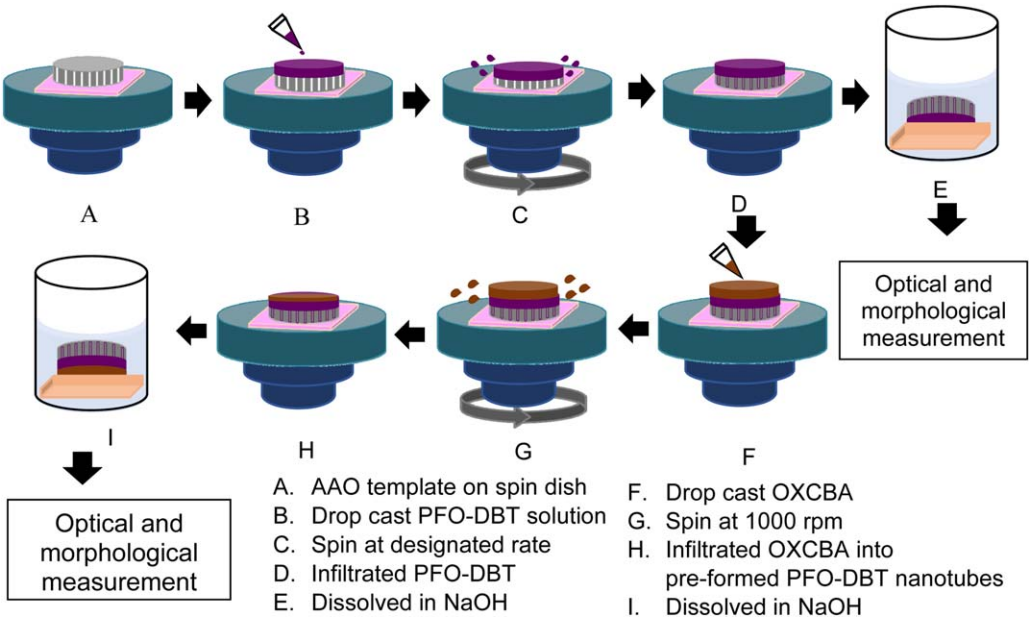

Figure 1. Schematic diagram of the experimental method. [Color figure can be viewed in the online issue, which is available at wileyonlinelibrary.com.]

coating rate of constant solution concentration has been reported.[25] However, at the constant spin rate, infiltration process will only be governed by the solution concentration since the constant spinning rate used will merely provide a similar behavior of polymer static and vibration. Relationship between the solution concentration and viscosity has previously been discussed by Durand[26] and Yang *et al.*[27] using the Huggins equation as shown in eq. (1).

$$\eta_{red} = [\eta] + \kappa_H [\eta]^2 C \quad (1)$$

From this equation, η_{red} is defined as the reduced viscosity that comprises of polymer solution and pure solvent viscosity. The intrinsic viscosity (η) is related to the specific volume of the macromolecules species that available within the solution. Interactions between solvent molecules and polymer solution macromolecular species are given by the Huggins coefficient (κ_H). From the Huggins equation, intrinsic viscosity (η) has a linear relationship with the solution concentration (c). Thus, increasing the polymer solution concentration could provide the higher solution viscosity which in the case of infiltration process, less or high viscous solution will infiltrate the nanoporous differently.

Figure 2(a) shows the FESEM image of PFO-DBT nanostructures produce from 5 mg/mL solution concentration via spin coating technique of constant spin rate. Shown by the enlarged FESEM image, gaps between the ensembles are huge at the concentration of 5 mg/mL. These gaps are corresponded to the no infiltration of PFO-DBT onto the nanochannels during the spin coating process. During the spin coating process, less viscous PFO-DBT solution is potentially thrown outward from the top surface of hard porous alumina template, which prevents the chances of intense infiltration. This phenomenon is occurred due to the higher exertion of centrifugal force produced by the spin coater on the less viscous solution. Once the spin coater is started to spin, the less viscous solution will easily get perturbed and spilled. As a result, gaps are appeared between the ensembles, which indicate the failure of infiltration. Different solution concentrations give different morphological behaviors on how the ensembles of PFO-DBT nanostructures grow. A solution with lower concentration will have a less viscous solution, which

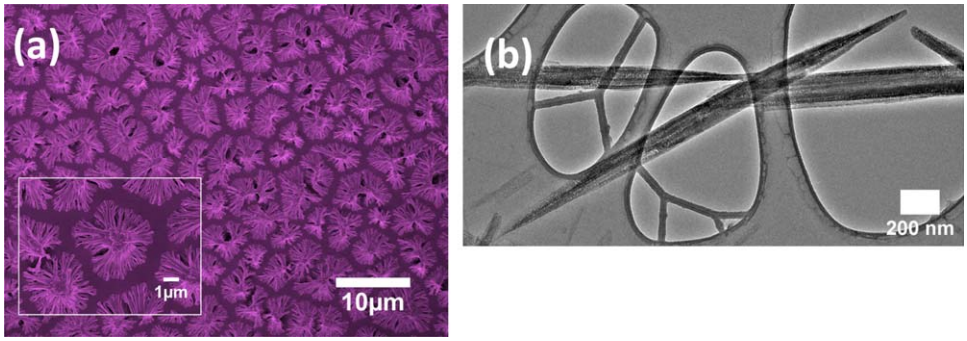

Figure 2. (a) FESEM image of PFO-DBT nanostructures and (b) HRTEM image of PFO-DBT nanorods fabricated at concentration of 5 mg/mL. [Color figure can be viewed in the online issue, which is available at wileyonlinelibrary.com.]

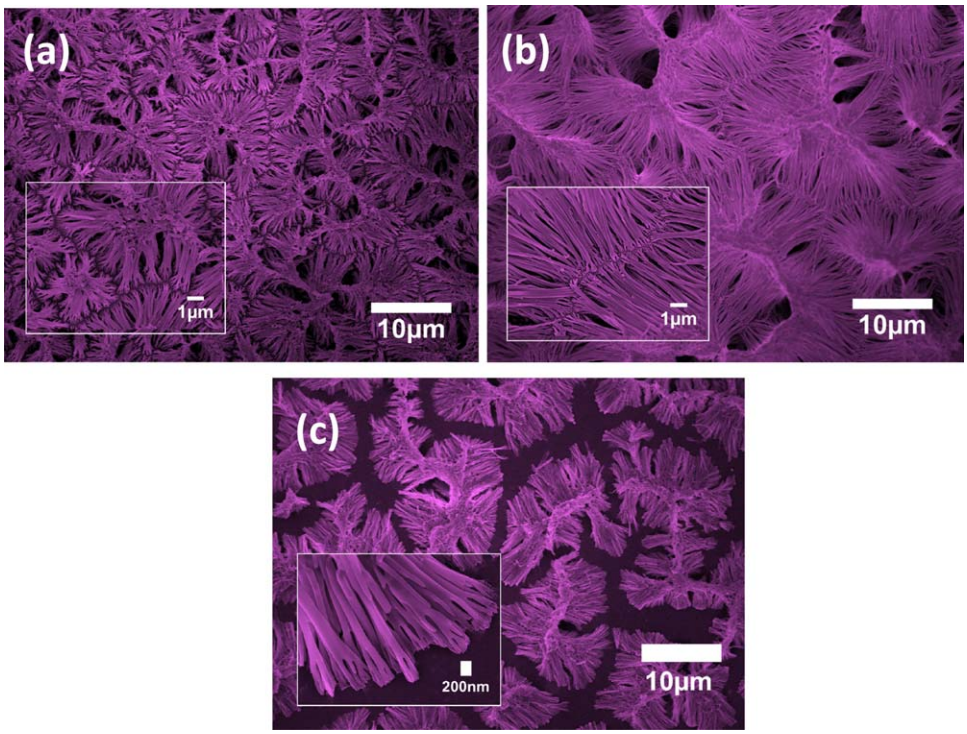

Figure 3. FESEM images of PFO-DBT nanostructures fabricated from (a) 10 mg/mL and (b) 15 mg/mL, (c) FESEM image of PFO-DBT:OXCBA nanostructured composite (inset shows the enlarged area of the ensembles). [Color figure can be viewed in the online issue, which is available at wileyonlinelibrary.com.]

could assist to the smooth flowing of solution inside the nanochannel. Fundamentally, less viscous solution is tending to favour the production of nanorods rather than other formation due to the strong proportional relation between solution concentration and viscosity.

Formation of nanorods from the less viscous solution could be due to the prompt evaporation of infiltrated PFO-DBT solution. As mentioned earlier, less viscous PFO-DBT solution has succeeded to infiltrate the nanochannel but not as a whole. The infiltrated PFO-DBT solution has experienced the smoother flow until at certain point it becomes saturated and solidified in the solid formation. TEM image shown in Figure 2(b) confirms the formation of PFO-DBT nanorods from the lower solution concentration of 5 mg/mL. Instead of only coating the nanoporous wall, which normally happened during the solution infiltration, the less viscous solution is capable to evaporate promptly and solidified thus form nanorods. The fabrication of PFO-DBT:OXCBA nanostructured composite can only be achieved when the OXCBA is incorporated with PFODBT. Since there are no hollow spaces within the nanorods, OXCBA is predicted to have difficulties in incorporating with PFO-DBT to forming the nanostructured composite materials.

The transition of formation from nanorods to nanotubes can be realised by increasing the solution concentration since it possesses a linear relationship with the viscosity. Therefore, at the higher solution concentration, adverse effect in the flowing of solution is experienced by the PFO-DBT solution due to the occurrence of higher solution viscosity. High viscous polymer solution will allow the solvent to evaporate slowly and give the opportunity for the solution to coat the nanoporous wall instead of solidified instantly in the middle of nanochannel as in the case of the less viscous PFO-DBT solution.

FESEM images of PFO-DBT nanostructures of higher solution concentration of 10 and 15 mg/mL are depicted in Figure 3(a,b), respectively. In contrast with Figure 2(a), no huge gaps are being produced by the high viscous polymer solution, at which the solution is hardly being thrown out from the template's surface. The gaps between the ensembles are reduced which suggest to a betterment of PFO-DBT infiltration when using a higher concentration of PFO-DBT solution. Formation transition of structure from nanorods to nanotubes has occurred by varying the solution concentration and thus its viscosity behavior. Formation of PFO-DBT nanotubes is realised from the concentration of 10 and 15 mg/mL. If comparison between the two different solution concentrations of 10 and 15 mg/mL is made, the former has the lengthy nanotubes than the latter due to the capability of 10 mg/mL of PFO-DBT solution to infiltrate deeper within the stimulated time to produce longer nanotubes.

For the fabrication of nanostructured composite material, the PFO-DBT nanotube has been chosen as a shell to allow the core of OXCBA solution to infiltrate and form the core-shell nanostructured composite. If PFO-DBT nanorods are used as a shell, one could expect that more efforts have to be put to infiltrate the OXCBA solution since not much porous areas are available within the nanorods. Figure 3(c) shows the FESEM images of PFO-DBT:OXCBA nanostructured composite that has been fabricated from the presynthesized PFO-DBT nanotubes of 10 mg/mL. Compared to the FESEM images of PFO-DBT

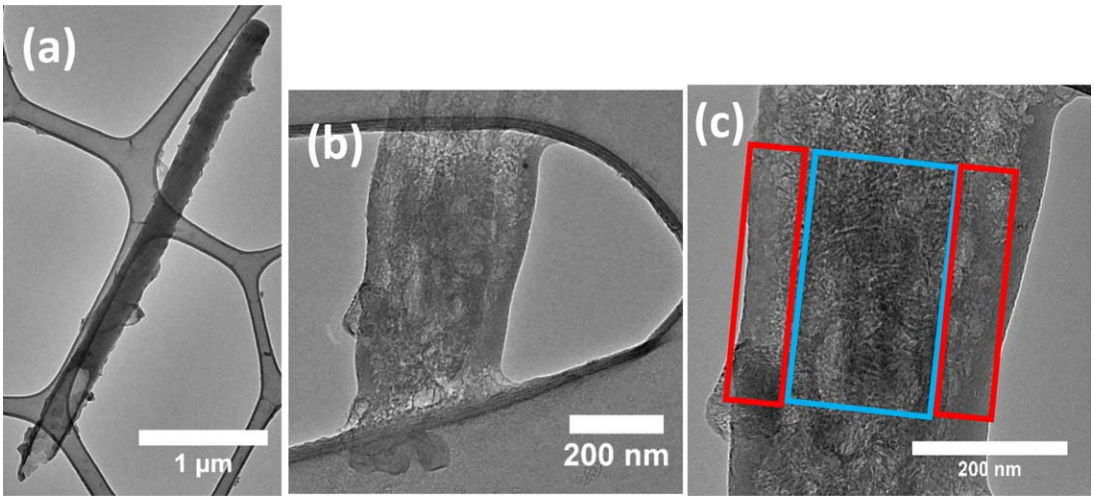

Figure 4. (a) HRTEM of individual PFO-DBT nanotube. (b) HRTEM image of individual PFO-DBT nanostructured composite, (c) HRTEM image showing the core-shell nanostructured composite. [Color figure can be viewed in the online issue, which is available at wileyonlinelibrary.com.]

nanotubes, FESEM images of nanostructured composite material show a different morphological distribution and length. The gaps between the ensembles are distinct in which the distribution of ensembles become lesser and the length of nanostructured composite become shorter. Since the similar solvent is used for both PFO-DBT and OXCBA solution, some of the PFO-DBT nanotubes may have been dissolved by OXCBA. Minor dissolution by OXCBA has cleared out the base structure of PFO-DBT nanotubes, which lead to the occurrence of gaps between ensembles. The thinner part of PFO-DBT nanotubes wall may have been also dissolved by OXCBA during infiltration, which cause the breakage and shorter nanostructured composite material.

PFO-DBT nanostructures of all concentrations have similarity on how the nanostructures are standing after template removal. Obviously, they are not standing straight upright but collapsed and leaned between the nanotubes at some point. These conditions have caused to the occurrence of nanostructures ensemble. Furthermore, the tips of each nanostructure are favoured to lean with each other and forming an aggregation. These formations happened due to the van der Waals force and strong surface tension at the interfaces during solvent evaporation. In addition, the other factor that contributes to this matter is the high aspect ratio (length to diameter) of nanostructures, which could cause to the collapsing of nanorods and nanotubes.

Figure 4(a) shows the TEM image of individual PFO-DBT nanotube fabricated from 10 mg/mL of PFO-DBT solution. HRTEM image shows the identical diameter size (~200 nm) of nanotubes that shown in FESEM image, which supported the existence of nanotubes at elevated concentration. From these images, it therefore suggests that the production of nanotubes can be realised from the hard templating method of spin coating technique. The wetting of solution onto nanoporous wall will lead to the formation of hollow space inside the nanochannel, which likely to result in the production of nanotube after template dissolution. Infiltration of OXCBA into the presynthesized PFO-DBT nanotube can be considered successful due to the formation of core-shell nanostructured composite as shown in HRTEM images [Figure 4(b,c)]. The inner solid core is corresponded to OXCBA due to the appearance of visible domains of molecules aggregation and arrangement (blue rectangular) while the outer shell (red rectangular) is indicated as PFO-DBT.

Figure 5(a,b) show the schematic diagram of nanoporous template before infiltration process and after the infiltration of high viscous PFO-DBT solution, respectively. The hard porous alumina template can be used as moulder to fabricate PFO-DBT nanotubes in which no adverse reaction between it and PFO-DBT solution is observed. Therefore, the consistency of yielding the PFO-DBT nanotubes may have been expected via the hard templating method. The consistency of the yielded nanostructures demonstrates that the PFO-DBT solution is successful in infiltrating and replicating the hard porous alumina template. Schematic diagram of PFO-DBT with solid inner core OXCBA wrapped by shell PFO-DBT is shown in Figure 5(c).

Optical Properties of PFO-DBT Nanostructures and PFO-DBT:OXCBA Nanostructured Composite

Figure 6(a) shows the absorption spectra of PFO-DBT nanostructures with the exhibition of two distinguish peaks. For all concentrations, the first peak that corresponds to B-band is absorbed at 385 nm. Based on the molecular structure of PFO-

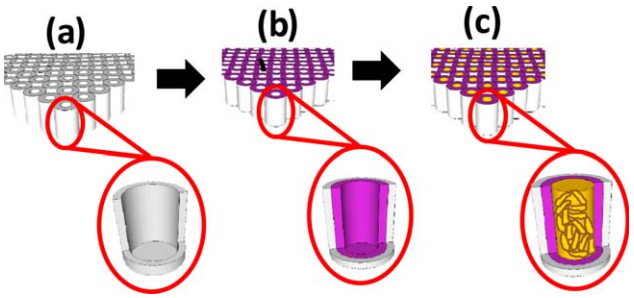

Figure 5. Schematic diagram of (a) hard porous alumina template and (b) PFO-DBT coated on porous wall and (c) schematic diagram of core OXCBA wrapped by shell PFO-DBT. [Color figure can be viewed in the online issue, which is available at wileyonlinelibrary.com.]

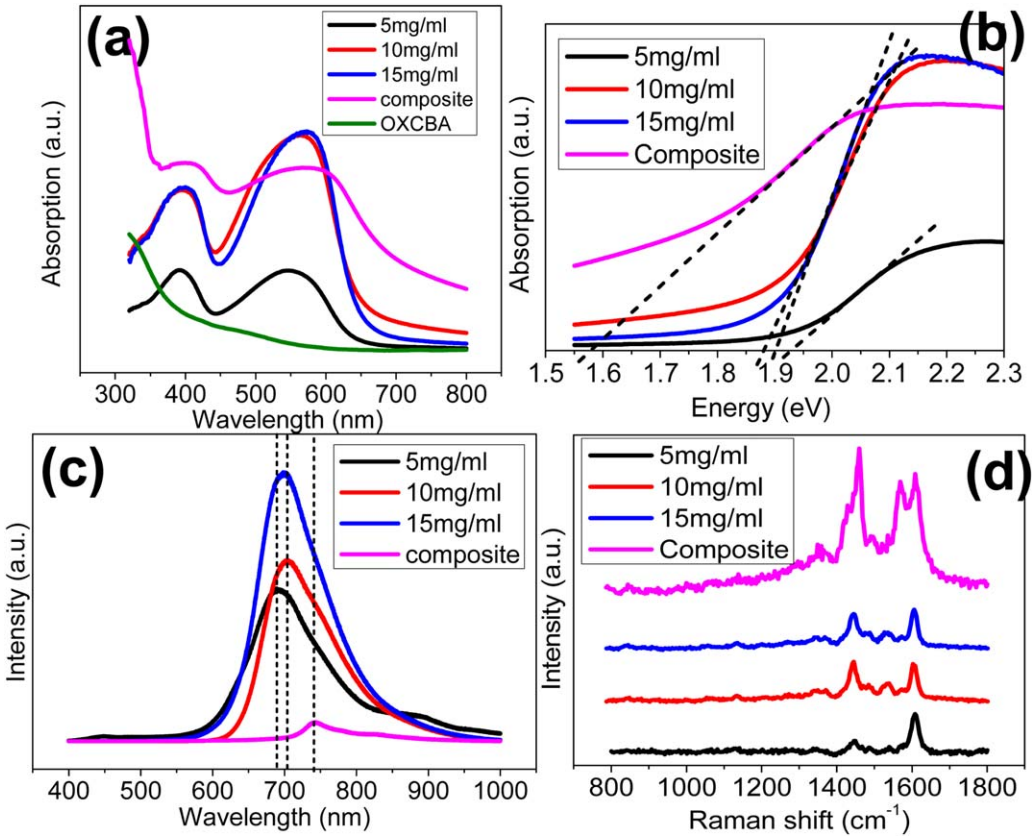

Figure 6. Optical properties of PFO-DBT nanostructures and PFO-DBT:OXCBA nanostructured composite of (a) UV-Vis absorption spectra, (b) optical energy gap [the dotted line is extrapolated from the absorption edge to intercept at *x*-axis], (c) photoluminescence spectra, and (d) Raman spectra of PFO-DBT nanostructure and PFO-DBT: OXCBA nanostructured composite. [Color figure can be viewed in the online issue, which is available at wileyonlinelibrary.com.]

DBT, at the UV region, light is absorbed mainly by the fluorene unit of PFO segment.[28] With the lesser gaps and denser distribution of PFO-DBT nanotubes that synthesized from concentration of 10 and 15 mg/mL, the light absorption at UV region become more intense which indicates a stronger and efficient π to π* transition. A denser morphological distribution could provide a higher surface area for the light to be absorbed. In the visible region, the light absorption has span around two-third of the region. Peak absorption at the visible region is due to the absorption by the thiophene unit in DBT segment.[29] As the solution concentration is varied, the peaks absorption and absorption edge are also varied. PFO-DBT nanostructures synthesized from 5 mg/mL exhibited B-band at 545 nm before being red-shifted to 577 nm with the increment of solution concentration (10 and 15 mg/mL). For OXCBA film, most of the light is absorbed at lower wavelength, which is similar to the absorption of light in PCBM film. Therefore, the UV-Vis absorption spectrum of PFO-DBT:OXCBA nanostructured composite material shows an additional high intensity absorption peak at the UV region that corresponds to the presence of OXCBA as a core material. Peaks absorption of PFO-DBT:OXCBA nanostructured composite in UV and visible regions has experienced the red shifting from 385 to 395 nm and 577 to 593 nm, respectively. Although the intensity of absorption is decreasing, the peak absorption of light is spanning almost the entire visible region. This phenomenon indicates that by integrating both PFO-DBT and OXCBA as nanostructured composite material, the light absorption of visible region can be enhanced.

Figure 6(b) shows the extrapolated graph from the edge of absorption to the *x*-axis, which gives the value of optical energy gap. The change in optical energy gap value corresponded to the broadness of absorption, which also influenced by the formation of PFO-DBT nanostructures and PFO-DBT:OXCBA nanostructured composite. Broader range of absorption is obtained from the PFO-DBT nanostructures fabricated from the higher solution concentration and even broader absorption can be achieved from the nanostructured composite material. A broader absorption range indicates the peak absorption at the longer wavelength and lower energy gap. Therefore, enhancing morphological properties of nanostructures is crucial since it is able to tune the optical energy gap. The broader absorption range is observed for PFO-DBT nanotubes (10 mg/mL) followed by PFO-DBT nanotubes of 15 mg/mL and PFO-DBT nanorods (5 mg/mL) with the optical energy gap of 1.87, 1.90, and 1.92 eV, respectively. Incorporation of OXCBA into PFO-DBT nanotube to form PFO-DBT:OXCBA nanostructured composite material has reduced the optical energy gap to 1.57 eV.

The quenching of peak intensity at the photoluminescence spectra indicates a better molecular arrangements and a better

Table I. Raman Peak Positions of PFO-DBT Nanostructures and PFO-DBT Nanostructured Composite Materials

Assignments	Raman shift (cm^{-1})	
	PFO-DBT	PFO-DBT: OXCBA
Ring breathing	732	732
Symmetric C=C=C stretch	844	844
CC stretches	1135	1135
CH deformation	1343	1343
CH_3 symmetric deformation	1367	1367
Ring stretch	1444	1444
Ring stretch	1481	1481
Antisymmetric NO_2 stretch	1536	1536
C=C stretch	1572	1572
Symmetric C=C stretch	-	1575
C=C stretch	1605	1605

photo-induced charge transfer within the materials.[30] However, Figure 6(c) demonstrates no quenching phenomena but increased in intensity as the solution concentration is increased. Low peak emission could be attributed to the less dense morphological distribution which likely to occur at the low solution concentration. The quenching of peak emission is recorded by the PFO-DBT:OXCBA nanostructured composite material which shown a better molecular arrangement that can be achieved with the incorporation of OXCBA. OXCBA has been able to infiltrate the PFO-DBT nanotube and allows the occurrence of photo-induced charge transfer between core-shell OXCBA:PFO-DBT nanostructured composite. PL emission peak of PFO-DBT nanostructures is shifted around ~20 nm from 680 nm (5 mg/mL) to 700 nm (10 and 15 mg/mL) while the peak emission of PFO-DBT:OXCBA nanostructured composite is shifted around ~65 nm. Red shifting is occurred at the edge of the PL emission peak, which is well correlated with the observation of red shifting at the peak and absorption edge of the UV-Vis absorption spectra.

The correlation between the intensity of photoluminescence and the molecular structure of PFO-DBT is discussed by analyzing the Raman spectra. Figure 6(d) shows the Raman spectra of PFO-DBT nanostructure and PFO-DBT: OXCBA nanostructured composite material. Their Raman peaks position and assignments are tabulated in Table I. There are not many changes at peak position that indicate the similar vibration of molecule in the molecular structure of PFO-DBT nanostructures. The only difference is the Raman intensity at 1444 cm^{-1} that is due to the vibration of ring stretching at the molecular structure. The intense Raman peak at 1444 cm^{-1} can be correlated with the higher detection of the irregular ring structure. The Raman peak intensity of 10 and 15 mg/mL at 1444 cm^{-1} is almost the same, which indicate the presence of similar quantity of ring structure. From the PL spectra, it is indicated that these rings are not having good molecular arrangement, as the peak intensity is not quenched if compared to the 5 mg/mL. However, PL peak intensity for 10 mg/mL is further quenched if compared with the 15 mg/mL, which suggest that the ring structure at 10 mg/mL has better molecular arrangement. Concentration of 10 mg/mL is more suitable to be used for the further fabrication of nanostructured composite materials.

From the Raman and PL spectra of nanostructured composite material, an intense Raman peak is observed and PL intensity is quenched, respectively. The presence of the respective molecular structure at each Raman shift is higher and based on the quenched phenomena of PL peak intensity, it suggested that the molecular structure is in good arrangement. Raman spectrum of PFO-DBT: OXCBA nanostructured composite material has exhibited an additional peak at 1575 cm^{-1}. This peak is corresponded to the vibration of symmetric C=C stretching which is the main component of OXCBA molecular structure. Therefore, the C=C stretching is mainly originated from carbon bond in the OXCBA. Other than its TEM image, these results prove the presence of OXCBA in the nanostructured composite material.

CONCLUSIONS

In this work, PFO-DBT nanostructures of different solution concentration have been synthesized using hard porous alumina template with the assistance of spin coating technique. Different morphological and optical properties of PFO-DBT nanostructures are obtained based on their initial solution concentration. At higher solution concentration, the infiltrated solution tends to form nanotube and acquire better light absorption and lower optical energy gap. Infiltrating OXCBA into the PFO-DBT nanotubes forms the PFO-DBT:OXCBA nanostructured composite material. Light absorption of PFO-DBT:OXCBA nanostructured composite has span over the visible region thus yielded the lower optical energy gap. PFO-DBT:OXCBA nanostructured composite material has achieved better molecular arrangement and improved photo-induced charge transfer.

ACKNOWLEDGMENTS

The authors acknowledge University of Malaya for project funding under University of Malaya Research Grant (RP026C-15AFR), Postgraduate Research Grant (PG058-2014A), and the Ministry of Education Malaysia for the project funding under the Fundamental Research Grant Scheme (FP046-2015A).

REFERENCES

1. Liu, X.; Sun, Y.; Hsu, B. B. Y.; Lorbach, A.; Qi, L.; Heeger, A. J.; Bazan, G. C. *J. Am. Chem. Soc.* **2014**, *136*, 5697.
2. Lee, K. H.; Schwenn, P. E.; Smith, A. R.; Cavaye, H.; Shaw, P. E.; James, M.; Krueger, K. B.; Gentle, I. R.; Meredith, P.; Burn, P. L. *Adv. Mater.* **2011**, *23*, 766.
3. Bronstein, H.; Chen, Z.; Ashraf, R. S.; Zhang, W.; Du, J.; Durrant, J. R.; Shakya Tuladhar, P.; Song, K.; Watkins, S. E.; Geerts, Y. *J. Am. Chem. Soc.* **2011**, *133*, 3272.
4. Gather, M. C.; Köhnen, A.; Meerholz, K. *Adv. Mater.* **2011**, *23*, 233.
5. Park, J. W.; Lee, D. H.; Chen, J.; Bae, M. H.; Kang, M. S.; Kim, Y. H.; Pyo, S.; Yi, M. H.; Kwon, S. K. *Curr. Appl. Phys.* **2010**, *10*, e152.

6. Kim, S. O.; Chung, D. S.; Cha, H.; Hwang, M. C.; Park, J. W.; Kim, Y. H.; Park, C. E.; Kwon, S. K. *Sol. Energy Mater. Sol. Cells* **2011**, *95*, 1678.
7. Umeyama, T.; Watanabe, Y.; Douvogianni, E.; Imahori, H. *J. Phys. Chem. C* **2013**, *117*, 21148.
8. Liu, L.; Li, H.; Yao, S.; Wei, Y.; Tian, W. *J. Mater. Sci.* **2015**, *50*, 57.
9. Schipper, D. J.; Fagnou, K. *Chem. Mater.* **2011**, *23*, 1594.
10. Liu, B.; Yu, W. L.; Lai, Y. H.; Huang, W. *Macromolecules* **2000**, *33*, 8945.
11. Dayal, S.; Kopidakis, N.; Olson, D. C.; Ginley, D. S.; Rumbles, G. *Nano Lett.* **2009**, *10*, 239.
12. Hou, J.; Chen, H. Y.; Zhang, S.; Chen, R. I.; Yang, Y.; Wu, Y.; Li, G. *J. Am. Chem. Soc.* **2009**, *131*, 15586.
13. Lin, L. Y.; Chen, Y. H.; Huang, Z. Y.; Lin, H. W.; Chou, S. H.; Lin, F.; Chen, C. W.; Liu, Y. H.; Wong, K. T. *J. Am. Chem. Soc.* **2011**, *133*, 15822.
14. Kim, K. H.; Kang, H.; Nam, S. Y.; Jung, J.; Kim, P. S.; Cho, C. H.; Lee, C.; Yoon, S. C.; Kim, B. *J.; Chem. Mater.* **2011**, *23*, 5090.
15. Kang, D. J.; Kang, H.; Cho, C.; Kim, K. H.; Jeong, S.; Lee, J. Y.; Kim, B. *J. Nanoscale* **2013**, *5*, 1858.
16. Marsh, R.; Groves, C.; Greenham, N. *J. Appl. Phys.* **2007**, *101*, 083509.
17. Chirvase, D.; Parisi, J.; Hummelen, J.; Dyakonov, V. *Nanotechnology* **2004**, *15*, 1317.
18. AlMawlawi, D.; Coombs, N.; Moskovits, M. *J. Appl. Phys.* **1991**, *70*, 4421.
19. Liu, H.; Sun, H.; Liu, L.; Hou, X.; Jia, X. *Opt. Mater.* **2015**, *44*, 9.
20. Kamarundzaman, A.; Fakir, M. S.; Supangat, A.; Sulaiman, K.; Zulfiqar, H. *Mater. Lett.* **2013**, *111*, 13.
21. Zakaria, R.; Hamdan, K. S.; Noh, S. M. C.; Supangat, A.; Sookhakian, M. *Opt. Mater. Expr.* **2015**, *5*, 943.
22. Haberkorn, N.; Gutmann, J. S.; Theato, P. *ACS Nano* **2009**, *3*, 1415.
23. Cao, G.; Liu, D. *Adv. Colloid Interface Sci.* **2008**, *136*, 45.
24. Tao, F.; Guan, M.; Jiang, Y.; Zhu, J.; Xu, Z.; Xue, Z. *Adv. Mater.* **2006**, *18*, 2161.
25. Fakir, M. S.; Supangat, A.; Sulaiman, K. *Nanoscale Res. Lett.* **2014**, *9*, 225.
26. Durand, A. *Eur. Polym. J.* **2007**, *43*, 1744.
27. Yang, H.; Yan, Y.; Zhu, P.; Li, H.; Zhu, Q.; Fan, C. *Eur. Polym. J.* **2005**, *41*, 329.
28. Ariu, M.; Lidzey, D. G.; Bradley, D. D. C. *Synth. Met.* **2000**, *607*, 111.
29. Huang, F.; Hou, L.; Shen, H.; Jiang, J.; Wang, F.; Zhen, H.; Cao, Y. *J. Mater. Chem.* **2005**, *15*, 2499.
30. Wang, J.; Wang, D.; Miller, E. K.; Moses, D.; Bazan, G. C.; Heeger, A. *J. Macromolecules* **2000**, *33*, 5153.